Distribution of High-Conductance Ca^{2+}-Activated K$^+$ Channels in Rat Brain: Targeting to Axons and Nerve Terminals

Hans-Günther Knaus,[1] Christoph Schwarzer,[2] Robert O. A. Koch,[1] Andreas Eberhart,[1] Gregory J. Kaczorowski,[3] Hartmut Glossmann,[1] Frank Wunder,[4] Olaf Pongs,[5] Maria L. Garcia,[3] and Günther Sperk[2]

[1]Institut für Biochemische Pharmakologie, A-6020 Innsbruck, Austria, [2]Institut für Pharmakologie, Abteilung für Neuropharmakologie, A-6020 Innsbruck, Austria, [3]Department of Membrane Biochemistry and Biophysics, Merck Research Laboratories, Rahway, New Jersey 07065, [4]Institute of Cardiovascular and Arteriosclerosis Research, Pharma Research Centre, Bayer AG, D-42096 Wuppertal-Elberfeld, Germany, and [5]Zentrum für Molekulare Neurobiologie, Institut für Neurale Signalverarbeitung, D-20246 Hamburg, Germany

Tissue expression and distribution of the high-conductance Ca^{2+}-activated K$^+$ channel *Slo* was investigated in rat brain by immunocytochemistry, *in situ* hybridization, and radioligand binding using the novel high-affinity (K_d 22 pM) ligand [^{3}H]iberiotoxin-D19C ([^{3}H]IbTX-D19C), which is an analog of the selective maxi-K peptidyl blocker IbTX. A sequence-directed antibody directed against *Slo* revealed the expression of a 125 kDa polypeptide in rat brain by Western blotting and precipitated the specifically bound [^{3}H]IbTX-D19C in solubilized brain membranes. *Slo* immunoreactivity was highly concentrated in terminal areas of prominent fiber tracts: the substantia nigra pars reticulata, globus pallidus, olfactory system, interpeduncular nucleus, hippocampal formation including mossy fibers and perforant path terminals, medial forebrain bundle and py-ramidal tract, as well as cerebellar Purkinje cells. *In situ* hybridization indicated high levels of *Slo* mRNA in the neocortex, olfactory system, habenula, striatum, granule and pyramidal cell layer of the hippocampus, and Purkinje cells. The distribution of *Slo* protein was confirmed in microdissected brain areas by Western blotting and radioligand-binding studies. The latter studies also established the pharmacological profile of neuronal *Slo* channels. The expression pattern of *Slo* is consistent with its targeting into a presynaptic compartment, which implies an important role in neural transmission.

Key words: maxi-K channel; distribution; expression; pharmacology; iberiotoxin; antibodies; in situ hybridization; immunocytochemistry

Ion channels play key roles in translating ionic fluxes across cellular membranes into electrical impulses through their ability to interconvert electrical signals. K$^+$ channels represent the largest and most diverse group of ion channels and are present in essentially every neuronal cell type (Latorre et al., 1989). They can be subdivided into voltage-gated K$^+$ and Ca^{2+}-activated K$^+$ channels. Two major classes of Ca^{2+}-activated K$^+$ channels have been identified in the CNS: (1) voltage-sensitive high-conductance (maxi-K) channels, most of which are blocked by charybdotoxin (ChTX) and iberiotoxin (IbTX) (Miller et al., 1985; Galvez et al., 1990); and (2) voltage-insensitive small-conductance channels, many of which are blocked by apamin (Lancaster et al., 1991).

The maxi-K channel has been purified from bovine tracheal smooth muscle (Garcia-Calvo et al., 1994) and is composed of two distinct subunits, α and β, (Knaus et al., 1994a). The α subunit is a member of the *Slo* family of K$^+$ channels, whereas the β subunit is a novel protein that has pronounced effects on the biophysical and pharmacological properties of the α subunit (McManus et al., 1995). Cloning of *Slo* channels from neuronal tissues has suggested the existence of a large number of channel isoforms (Butler et al., 1993; Tseng-Crank et al., 1994). This diversity is generated by alternative RNA splicing of a single gene (Butler et al., 1993; Dworetzky et al., 1994; Pallanck and Ganetzky, 1994). Alternatively spliced constructs differ significantly in their biophysical properties (Adelman et al., 1992; Tseng-Crank et al., 1994; Wei et al., 1994). Thus, alternative RNA splicing, opposite regulation via phosphorylation by various protein kinases, and perhaps association with other accessory subunits could contribute to the diversity of *Slo* channels in mammalian brain (Reinhart et al., 1989, 1991; Tseng-Crank et al., 1994). The functional role of *Slo* channels in the mammalian brain is not well understood. Their putative colocalization with voltage-gated Ca^{2+} channels suggests that they function as feedback regulators of intracellular Ca^{2+} concentration by hyperpolarizing the plasma membrane (Robitaille and Charlton, 1992). In some neurons, this may allow *Slo* channels to regulate the amount of neurotransmitter released from presynaptic nerve terminals by modulating the duration of the presynaptic action potential (Robitaille et al., 1993). Additionally, these channels can also contribute to firing patterns (MacDermott and Weight, 1982) and afterhyperpolarization in certain neurons (Lancaster and Nicoll, 1987).

To obtain a better understanding of the functional role of this channel, detailed knowledge regarding its regional distribution and cytological localization is required. Sequence-directed anti-

peptide antibodies against a conserved region of Slo have been raised and used in immunocytochemical studies. Perikarya expressing Slo were identified by in situ hybridization. Slo immunoreactivity at the protein level from different rat brain regions was characterized in Western blots. Radioligand binding and immunoprecipitation studies with a tritiated IbTX analog were used to confirm the distribution pattern of the channel and to establish its pharmacological characteristics.

MATERIALS AND METHODS

Materials. Affinity-purified alkaline phosphatase-conjugated goat anti-rabbit IgG, nitro blue tetrazolium, 5-bromo-4-chloro-3-indoyl phosphate, Tween 20, and Triton X-100 were obtained from Sigma (Diesenhofen, Germany). Cyanogen bromide-activated Sepharose was obtained from Pharmacia (Uppsala, Sweden). Prestained molecular mass standards (range 14.4–106 kDa) and Immobilon polyvinylidene difluoride membranes were obtained from Bio-Rad (Richmond, CA). All other reagents were of the highest purity grade commercially available. *Escherichia coli* DH5α was used for plasmid propagation, and strain BL21(DE3) was used for expression of the fusion protein. Plasmid PGEMEX-1 was from Promega (Madison, WI). Terminal desoxynucleotidyl transferase and quick-spin columns were from Boehringer Mannheim (Mannheim, Germany). [α-^{33}P]dATP and Enlightning were from DuPont NEN (Boston, MA). Hyperfilm βmax was purchased from Amersham (Buckingham-shire, UK).

Antibody production. A polyclonal serum was raised against residue positions 913–926 of Slo (Butler et al., 1993) using the sequence VNDT-NVQFLDQDDD (anti-α$_{(913-926)}$). The immunogenic peptide was synthesized on a lysine core linked to a solid-phase peptide synthesis support. After cleavage, 2 μmol of peptide emulsified in complete Freund's adjuvant was injected into two rabbits. The procedure was repeated 1 month later, and serum was collected 2 weeks later. Antibody production was monitored by ELISA following standard protocols. Antibodies drawn 12–16 weeks after primary immunization were used for all experiments presented.

Affinity purification of anti-α$_{(913-926)}$ and immunoblot analysis. The peptide VNDTNVQFLDQDDD (2 μmol) was dissolved in 100 mM NaHCO₃ buffer, pH 8.5, and incubated with 1 gm of cyanogen bromide-activated Sepharose (4 ml of packed gel) for 12 hr at 4°C. The coupling efficiency was monitored by determining the absorbance at 215 nm before and after coupling. Thereafter, the affinity matrix was washed alternately with (500 ml each) 50 mM ammonium acetate, pH 4.0, and 50 mM Tris-HCl, pH 8.5, and equilibrated with 20 mM Tris-HCl, pH 7.4, and 150 mM NaCl (TBS). Crude serum (3 ml) was incubated under gentle rotation with the affinity matrix for 12–15 hr at 4°C. After unbound material was collected and the gel was washed with TBS, antibodies were eluted within 5 min with either 100 mM glycine buffer, pH 2.5, or 5 M MgCl₂. The glycine buffer was neutralized immediately with 2 M Tris base, and the MgCl₂ eluate was diluted fivefold with ice-cold TBS and 1 mg/ml bovine serum albumin (BSA) and washed several times with ice-cold TBS in a Centricon-30 device (Amicon, Beverly, MA). The overall recovery, as determined by ELISA, was usually 20–40%. The antibody aliquots were stored at −20°C in 20 mM Tris-HCl, pH 7.4, 150 mM NaCl, and 0.02% NaN₃, without any loss in activity. Immunoblot analysis, in vitro translation of Slo, and immunoprecipitation studies were performed as described in detail in Knaus et al. (1995).

Immunocytochemistry. Male Sprague–Dawley rats (300–500 gm) were injected with a lethal dose of thiopental (150 mg/kg, i.p.). Their brains were perfused via the ascending aorta with 50 ml of ice-cold saline (0.9%) buffered with 50 mM phosphate, pH 7.4, followed by 250 ml of chilled 4% p-formaldehyde in PBS (as above). After dissection, the brains were blocked into three parts, post-fixed for 90 min in the same fixative, transferred to 20% sucrose in PBS, and kept there for 24 hr (both at 4°C). Thereafter, brains were flash-frozen in isopentane (−70°C) for 3 min. The brains were kept in air-tight vials at −70°C. Before use, the brains were cut into 40 μm sections.

The indirect peroxidase–antiperoxidase technique (Sternberger, 1979) was used with free-floating slices, as described previously (Marksteiner et al., 1992). In brief, sections were incubated 72–96 hr in 50 mM Tris-HCl, pH 7.4, 0.85% NaCl, 0.4% Triton X-100, 0.1% NaN₃, 2% ovalbumin, and 2% normal goat serum with affinity-purified anti-α$_{(913-926)}$ to a dilution of 1:3000 of the original serum. Immunoreaction products were visualized by coupling with rabbit peroxidase–antiperoxidase via goat anti-rabbit

IgG and color reaction with 3,3-diaminobenzidine. In control sections, nonspecific immunoreactivity was assessed by preadsorbing anti-α$_{(913-926)}$ with 10 μM of the respective peptide and by incubation without the primary antibody.

In situ hybridization. For detection of the Slo transcript, two antisense oligonucleotides were synthesized on a DNA synthesizer (Applied Biosystems, Foster City, CA). Probes were taken from the C-terminal domain. The following oligonucleotides were synthesized complementary to the Slo sequence [(Butler et al., 1993) accession number L16912]: nt 1351–1400 (TTG GAG GCA TCT TCT GCA TCC GGG TCA GCG CAA TAC TTA TTG GCA AGG AT), and nt 3180–3229 (CTG TTG GTA CGA GCT CAA ACT CGT AGG GAG GAT TGG TGA TGA CGT ACC TT); each gave essentially identical results. A sense oligonucleotide was used as a negative control; the control experiments showed no specific hybridization signals (data not shown). In situ hybridizations were performed according to Wisden et al. (1990). Probes were labeled at the 3' ends with terminal desoxynucleotidyl transferase and [α-^{33}P]dATP (1000–3000 Ci/mmol) to a specific activity of 10⁹ dpm/μg. Unincorporated nucleotides were removed by quick-spin columns.

For in situ hybridization, brains were obtained from nonperfused rats and rapidly frozen on dry ice. Sections (16 μm) were cut on a cryostat, thaw-mounted onto silane-coated slides, air-dried, and fixed in 4% p-formaldehyde. After washing in PBS, sections were dehydrated and stored under ethanol at 4°C. Labeled probes were dissolved in hybridization buffer (5000 dpm/μl) and then applied to the air-dried sections. Hybridization buffer contained 50% formamide, 10% dextran sulfate, 0.3 M NaCl, 30 mM Tris-HCl, pH 7.7, 4 mM EDTA, 5 × Denhardt's solution, 25 mM dithiothreitol (DTT), 0.5 mg/ml yeast tRNA, and 0.5 mg/ml denatured salmon sperm DNA. The hybridizations were performed overnight at 42°C. Sections were washed to a final stringency of 1× SSC at 58°C, dehydrated, and exposed to Hyperfilm βmax for 3 weeks. Some sections were dipped into Kodak NTB2 nuclear track emulsion, exposed for 6 weeks at 4°C, developed with Kodak D19 developer, and counter-stained with cresyl violet. Brain structures were identified using a brain atlas (Paxinos and Watson, 1986).

Preparation of purified synaptic plasma membrane vesicles from rat brain. Rats (Wistar, 150–250 gm) were decapitated, their brains were dissected rapidly, and the tissue was placed in ice-cold homogenation buffer (320 mM sucrose, 1 mM K₂-EDTA, and 10 mM Tris-HCl, pH 7.4). Synaptic plasma membrane vesicles were prepared by a method published previously (Vázquez et al., 1990). Membrane vesicles were resuspended in 50 mM Tris-HCl, pH 7.4, flash-frozen in liquid nitrogen, and stored at −80°C. Under these conditions, binding was stable for at least 6 months.

Expression and purification of recombinant IbTX-D19C. The plasmid pG9IbTX, encoding six histidine residues between the fusion protein and the factor Xa cleavage site and the wild-type IbTX sequence, was constructed in the following manner. The BamHI–HindIII fragment from p6HisMgTX (Johnson et al., 1994) was excised and subcloned into PGEMEX-1, and the Gene 10 sequence was removed with SmaI/BamHI and replaced with the Gene 9 sequence excised from pMgTX (Garcia-Calvo et al., 1993). The MgTX sequence was then replaced by IbTX to generate pG9IbTX. This plasmid was altered such that codon 19 of IbTX was transformed from aspartic acid to cysteine (Cys). The fusion protein was expressed in E. coli and purified essentially as described previously (Garcia-Calvo et al., 1993). Fractions containing the fusion protein were identified by Coomassie staining of SDS-PAGE gels, combined, and dialyzed overnight against 20 mM Tris-HCl, 100 mM NaCl, and 0.5 mM β-mercaptoethanol, pH 8.3. CaCl₂ was then added to a final concentration of 3 mM, and 1 μg of Factor Xa was added per milligram of fusion protein. The mixture was incubated at room temperature for 18 hr, dialyzed against 20 mM sodium borate, pH 9.0, and loaded onto a Mono-S HR10/10 cation-exchange chromatography column (Pharmacia) equilibrated with 20 mM sodium borate, pH 9.0. Elution of bound material was achieved in the presence of a linear gradient of NaCl (0–500 mM NaCl, 60 min) at a flow rate of 2 ml/min. The fraction containing recombinant IbTX-D19C was identified by N-terminal sequencing and incubated with 5% acetic acid at 45°C for 48 hr. This incubation time was required to achieve full cyclization of the N-terminal residue. Then the sample was applied to a C₁₈ reversed-phase HPLC column, and elution was carried out using conditions similar to those reported previously for native IbTX (Galvez et al., 1990). Composition of the purified material was verified by electrospray mass spectroscopy and Edman degradation. Aliquots were lyophilized and stored at −80°C.

Labeling of recombinant IbTX-D19C with N-[³H]ethylmaleimide. IbTX-D19C (160 μg) in 50 mM sodium phosphate, pH 7.0, was incubated with

10 mM DTT for 1 hr at room temperature. The reaction mixture was applied to a C_{18} reversed-phase column (Vydac, Hesperia, CA; 0.45×25 cm^2) and eluted with a linear gradient of 10–30% isopropanol/acetonitrile (2:1) to purify IbTX-D19C with a free sulfhydryl group. The reduced toxin was concentrated to 20 μl, and 100 μl of 50 mM sodium phosphate was added. This solution was added to 200 μl of 89 μM N-[1,2-^{3}H]ethylmaleimide in 50 mM sodium phosphate, pH 7.0, and the mixture was incubated at 37°C for 1 hr. The reaction products were separated by reversed-phase chromatography on a C_{18} column using the same elution conditions as indicated above for IbTX-D19C-SH. The radiolabeled peptide was resuspended in 100 mM NaCl, 20 mM Tris-HCl, pH 7.4, and 0.1% BSA and stored at -20°C.

Solubilization of Slo *channels, binding studies with recombinant [^{3}H]IbTX-D19C, and analysis of data.* Neuronal *Slo* channels were prelabeled with [^{3}H]IbTX-D19C for 12 hr at room temperature and solubilized as described previously (Garcia-Calvo et al., 1994).

For radioligand binding studies with [^{3}H]IbTX-D19C and rat brain membranes, the incubation medium (4 ml) consisted of 10 mM NaCl, 20 mM Tris-HCl, pH 7.4, and 0.1% BSA (buffer A). Nonspecific binding was defined in the presence of 10 nM synthetic ChTX, and incubation was carried out at 22–25°C, typically overnight. All serial toxin dilutions were performed in a BSA-containing buffer and added directly to the incubation mixture to avoid adsorption phenomena. At the end of incubation, the reaction mixture was filtered rapidly through Whatman GF/C glass fiber filters (Maidstone, UK) that had been presoaked for at least 60 min in 0.3% (w/v) polyethyleneimine, followed by two washes with ice-cold filtration buffer (20 mM Tris-HCl, pH 7.4, 150 mM NaCl; 4 ml/wash). With this protocol and at a K_d concentration of radioligand and receptor, nonspecific binding represented <3% of the total amount of radioactivity added, and specific binding was >95% of total binding. Duplicate or triplicate assays were routinely performed in each experiment, and data were averaged. The results from saturation binding experiments were subjected to a Scatchard analysis, and linear regression was performed to obtain the equilibrium dissociation constant (K_d) and maximal receptor concentration (B_{max}). To determine K_i values, data from competition experiments were computer-fitted to the general dose–response equation (DeLean et al., 1978) and then analyzed by a method described previously (Linden, 1982).

SDS-PAGE, protein determination, and autoradiography. Standard SDS-PAGE was carried out as described previously (Laemmli, 1970). Prestained molecular weight standards were used to generate standard curves from which the M_r of the fragments was calculated by nonlinear regression analysis. Protein concentration was determined according to Bradford (1976) using BSA as standard. To visualize the [^{35}S]methionine-labeled translation product of *Slo*, the gels were incubated with Enlightning reagent according to the protocol of the manufacturer and developed overnight on a PhosphoImager (Molecular Dynamics, Sunnyvale, CA).

RESULTS

Characterization of a *Slo*-specific antibody in immunoblot analysis of rat brain

Anti-$\alpha_{(913-926)}$, a sequence-directed antibody directed against the pore-forming α subunit of the maxi-K channel, also referred to as *Slo*, was applied to investigate the presence and apparent molecular weight of the tissue-expressed gene product of *Slo*. Anti-$\alpha_{(913-926)}$ specifically recognized the *in vitro* translated *Slo* protein in immunoprecipitation assays (Fig. 1*A*, *lanes a* and *b*). More important, this antibody stained a singular diffuse band in rat brain membranes, which probably consisted of multiple partially resolved components, with an overall molecular mass of 125 kDa (Fig. 1*A*, *lanes c* and *f*, *B*). In immunoblotting experiments using membranes derived from different brain regions, the highest levels of *Slo* immunoreactivity were found in substantia nigra and the hippocampal formation (Fig. 1*B*, *lanes c* and *f*). High levels of *Slo* protein were also detected in the frontal cortex, olfactory tubercle, striatum, globus pallidus, and cerebellum (Figs. 1*A*, *lanes c* and *f*, 2). Significantly lower channel levels were seen in the brain stem and the spinal cord. Immunostaining of this polypeptide was
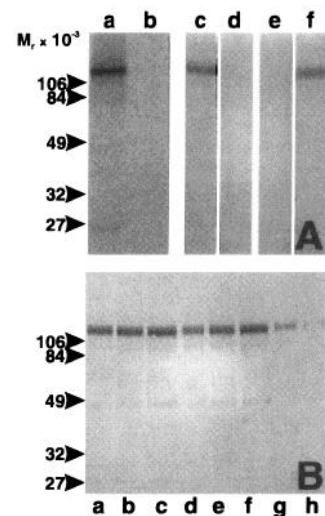

Figure 1. Immunological identification of *Slo* in rat brain membranes. *A*, Immunoprecipitation of the [^{35}S]methionine-labeled *in vitro* translation product of *Slo*. Immunoprecipitation studies using anti-$\alpha_{(913-926)}$ in the absence (*lane a*) and presence (*lane b*) of 3 μM competitor peptide. Rat neocortex (*lanes c* and *d*) and cerebellar (*lanes e* and *f*) synaptic plasma membrane vesicles were separated by 12% SDS-PAGE under reducing conditions and immunoblotted using anti-$\alpha_{(913-926)}$ in the absence (*lanes c* and *f*) and presence (*lanes d* and *e*) of 1 μM competing peptide. Tissue-expressed *Slo* protein was recognized as a diffuse band of M_r 125 kDa. *B*, Immunoblotting using anti-$\alpha_{(913-926)}$ of rat brain synaptic plasma membrane vesicles after microdissecting the respective brain regions. *Lane a*, frontal cortex; *lane b*, olfactory tubercle; *lane c*, hippocampus; *lane d*, striatum; *lane e*, globus pallidus; *lane f*, substantia nigra; *lane g*, brain stem; *lane h*, spinal cord. The positions of molecular mass standards (in kDa) are depicted.
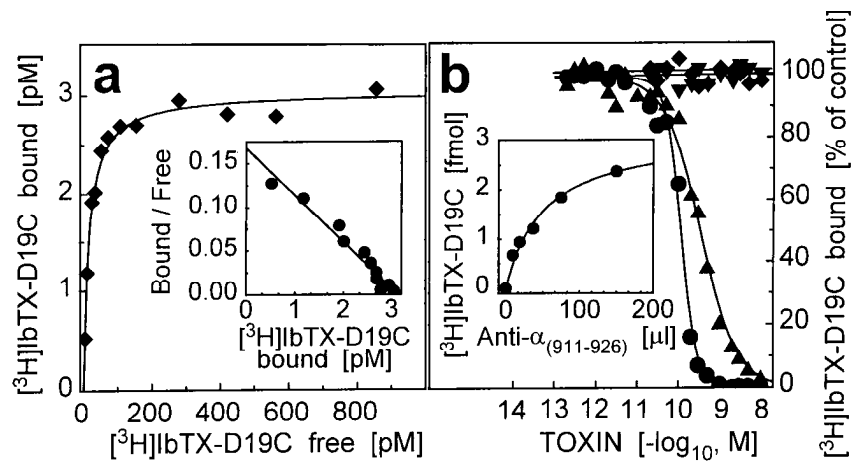
completely abolished in the presence of 1 μM immunogenic peptide (Fig. 1, *lanes d* and *e*).

Quantification of *Slo* expression in rat brain

To quantify levels of tissue expression in mammalian brain and to investigate the pharmacological characteristics of maxi-K channels, we synthesized [^{3}H]IbTX-D19C, an analog of the maxi-K channel-selective peptidyl inhibitor IbTX. This ligand was characterized in binding studies with rat brain synaptic plasma membrane vesicles (Fig. 2). In this system, [^{3}H]IbTX-D19C binds to a single class of sites that displays a K_d of 22 pM with a maximum density of 0.13 pmol/mg protein (Fig. 2*a*). To determine the pharmacological properties of the binding reaction, various toxins that are known to interact specifically with K^+ channels were tested for their ability to modulate [^{3}H]IbTX-D19C binding. ChTX and IbTX completely inhibit binding of [^{3}H]IbTX-D19C to brain plasma membranes in a concentration-dependent manner, with K_i values of 23 pM and 59 pM, respectively. In contrast, margatoxin and α-dendrotoxin, blockers of voltage-gated K^+ channels, did not affect [^{3}H]IbTX-D19C binding at concentrations up to 10 nM (Fig. 2*b*).

To quantify levels of maxi-K channel expression in individual brain regions, binding of [^{3}H]IbTX-D19C was carried out with synaptic plasma membrane vesicles prepared from defined regions after rat brains were microdissected. Results from these experiments are presented in Table 1. All brain regions that were investigated bound [^{3}H]IbTX-D19C with dissociation constants ranging from 18 to 34 pM. The maximum density of binding sites, however, varied significantly. The highest density of sites was observed in the olfactory tubercle, the frontal cortex, and the

Figure 2. Binding properties of [³H]IbTX-D19C to *Slo* channels in rat brain synaptic plasma membrane vesicles. *a*, Saturation binding analysis. Rat brain synaptic plasma membrane vesicles (0.022 mg/ml) were incubated with increasing concentrations (4–855 pM) of [³H]IbTX-D19C. The binding reaction was carried out as described in Materials and Methods. Specific binding was assessed from the difference between total and nonspecific ligand binding. For this experiment, a K_d of 19 pM and a B_{max} value of 3.1 pM (corresponding to 0.14 pmol/mg protein) were measured. *Inset* shows specific binding data from *a* presented in the form of a Scatchard representation. *b*, Membrane vesicles (0.08 mg/ml) were incubated with 44 pM [³H]IbTX-D19C in the absence or presence of increasing concentrations of ChTX (●, IC_{50} = 89 pM, n_H = 2.2), IbTX (▲, IC_{50} = 212 pM, n_H = 1.02), α-DaTX (▼), or MgTX (♦) at 22°C until equilibrium was achieved. Inhibition of binding by these toxins was assessed compared with an untreated control. *Inset* shows immunoprecipitation of [³H]IbTX-D19C-labeled, digitonin-solubilized neuronal *Slo* channels by crude anti-α(913–926) serum immobilized on protein A-Sepharose; >2.5 fmol of solubilized maxi-K channels was precipitated, which corresponds to >28% of added receptor–ligand complex.

hippocampus. Less than 10% of this site density was detected in brain stem and spinal cord, which is in agreement with the distribution pattern of *Slo* protein, when these same membranes were probed in Western blots with anti-α(913–926) (see Fig. 1*B*). As an additional demonstration that the protein recognized by anti-α(913–926) is identical to the receptor labeled by [³H]IbTX-D19C, anti-α(913–926) was used in immunoprecipitation studies of digitonin-solubilized neuronal *Slo* channels. The digitonin-solubilized channel, prelabeled with [³H]IbTX-D19C, was specifically immunoprecipitated to a significant extent and in a dose-dependent manner by either crude anti-α(913–926) serum (Fig. 2*C*) or the affinity-purified antibody (data not shown).

Regional distribution of *Slo* immunoreactivity and mRNA in rat brain

Given the high specificity of anti-α(913–926) for *Slo* channels, the neuronal distribution pattern of these channels was investigated by parallel immunocytochemical analysis using this antibody and *in situ* hybridization studies. The results of these experiments are shown in Figures 3–5. In all instances, excess of immunogenic peptide completely abolished the staining reaction (data not shown). *Slo* immunoreactivity was found in individual somata and was also distributed diffusely in various brain regions. In all cases,

Table 1. Distribution of *Slo* channels in rat brain measured by [³H]IbTX-D19C binding

Rat brain tissue	[³H]IbTX-D19C binding B_{max} (pmol/mg protein)	K_d (pM)
Frontal cortex	0.191	36.7
Olfactory tubercle	0.163	29.3
Piriform cortex	0.125	26.7
Hippocampus	0.141	23.3
Striatum	0.099	23.8
Thalamus	0.059	20.1
Hypothalamus	0.029	19.1
Brain stem	0.018	25.8
Spinal cord	0.011	23.4

the *Slo* immunostaining pattern revealed typical anatomical patterns, which most likely reflect staining of neuronal fibers. The most intense immunoreactive staining was observed in target areas of defined fiber tracts, whereas individual immunoreactive fibers were identified only occasionally. *Slo* immunoreactivity was negligible in major white matter tracts (e.g., corpus callosum) and in glial cells.

Slo expression in the neocortex

Within the neocortex, the *Slo* antibody reveals staining of the neutropil in all regions and throughout the entire thickness of the cerebral cortex, although immunoreactivity was especially enriched in layers II and VI (Fig. 3*a,b*), which is where most of the *Slo*-positive neurons exhibit a shape and size typical for pyramidal neurons. This distribution correlates well with *in situ* hybridization data, which reveal high *Slo* mRNA levels in the neocortex, with particularly dense signals overlaying large cell bodies (presumably pyramidal cells). In accordance with these *in situ* hybridization results, prominent *Slo* immunoreactivity was present along the pyramidal tract in the brain stem, the major fiber system arising from pyramidal neurons of the cortex (Fig. 5*g*). Among other major projection areas of the neocortex, diffuse *Slo* immunoreactivity was detected in the neocortex itself, the striatum, the pontine nuclei (Fig. 5*d, arrow*), and the thalamic nuclei (Figs. 3*a,b*, 4*a,b*).

Slo expression in the hippocampus

High levels of *Slo* protein and mRNA are expressed in the hippocampal formation (Figs. 3*a*, 4*a–c*), which is consistent with previous electrophysiological data (Lancaster and Nicoll, 1987; Lancaster et al., 1991). *Slo* mRNA is highly concentrated in all principal neurons of the hippocampal formation. The corresponding protein is found partly within the same cell layers but is mostly targeted to the axonal compartment of these neurons. *Slo* immunoreactivity is expressed strongly in mossy fibers, which represent the axons of granule cells innervating CA3 pyramidal neurons. (Fig. 4*c*). Moreover, hippocampal *Slo* expression is observed in the middle and outer parts of the molecular layer, which suggests that the protein is contained within fibers of the perforant path terminating in this region of hippocampal formation. This fiber

Figure 3. Photographs of sagittal sections showing an auto-radiogram of *Slo* mRNA (*a*) and *Slo* immunoreactivity (*b*). Scale bar, 2 mm.

tract represents the major excitatory projection innervating the hippocampus. It originates from the entorhinal cortex in which high mRNA concentrations are detected. The presence of *Slo* immunoreactivity within the target areas of these hippocampal projections, in conjunction with the expression of *Slo* mRNA within CA3 and CA1 pyramidal neurons, suggests that maxi-K channels participate in major afferent, intrinsic, and efferent projections of the hippocampus. These neurons comprise an excitatory circuit of important physiological relevance, including long-term potentiation (Zalutsky and Nicoll, 1990; Madison et al., 1991), and are causally involved in the generation of temporal lobe epilepsy (Meldrum and Corsellis, 1984).

Slo expression in the olfactory system

Slo mRNA is found in perikarya of the primary olfactory sensory neurons in the nasal cavity (data not shown). The axons of these neurons enter the olfactory bulb surface through the olfactory nerve layer and terminate in the glomerular layer in regions of neutropil called "glomeruli." Both layers are strongly stained with the *Slo* antibody (Fig. 4*d*). Within the olfactory bulb, strong *in situ* hybridization signals are found overlaying mitral and granule cells located in the respective cell layers in the depths of the olfactory bulb (Figs. 3*a*, 4*b*). Some *Slo* immunoreactivity is associated here with mitral and granule cell somata, an observation that is in accordance with the electrophysiological demonstration of *Slo* channels on cell bodies of olfactory bulb neurons (Egan et al., 1993).

The dendrites of mitral cells, the secondary olfactory sensory neuron, traverse the external plexiform layer to terminate within the superficially located glomeruli, thereby forming axo-dendritic contacts with the primary olfactory axon. The external plexiform layer, which contains dendrites of mitral and granule cells exclusively, is essentially devoid of *Slo* immunoreactivity. In striking contrast, the central olfactory bulb layers (the mitral cell, the inner plexiform, and the granule cell layer) express high levels of *Slo* immunoreactivity. There the axons of mitral cells proceed into the very center of the olfactory bulb to reach their target areas in the

olfactory cortex, which is also highly immunoreactive (data not shown). In summary, the axonal and presynaptic compartments of the primary and secondary olfactory sensory neurons express high levels of *Slo* channels, whereas the external plexiform layer, an exclusively dendritic compartment, is devoid of *Slo* immunoreactivity.

Slo expression in the extrapyramidal system

Within the basal ganglia, *Slo* immunoreactivity is concentrated in three closely related structures: the globus pallidus, the substantia nigra pars reticulata, and the entopeducular nucleus. The corresponding mRNA is not found in these regions, however, but is concentrated instead over the striatum (Fig. 3*a*), a brain region that contributes dense projections to the globus pallidus (Fig. 4*e*), the substantia nigra pars reticulata (Figs. 4*f*, 5*d*), and the entopeducular nucleus (Fig. 4*h*) (Heimer et al., 1995). In contrast, the substantia nigra pars compacta (which gives rise to dopaminergic neurons projecting to the striatum) is devoid of *Slo* immunoreactivity and mRNA (Fig. 4*f*). The most likely explanation for this illustrative anatomical distribution of *Slo* channels within the basal ganglia is that the *Slo* protein is being synthesized in projecting neurons within the striatum but is subsequently transported down their axons to be concentrated in nerve terminals of the respective fiber tracts. In accordance with these data, a high level of *Slo* immunoreactivity is detected in a major neuroanatomically well defined fiber tract connecting some of these brain regions, the medial forebrain bundle (Fig. 4*g*).

Slo expression in the habenula and interpeduncular nucleus

Among the regions with the highest concentration of *Slo* mRNA is the medial habenula (Figs. 4*a*, *arrow*, 5*a*), but only low levels of the corresponding protein can be detected in this nucleus. *Slo* immunoreactivity is observed along the entire fasciculus retroflexus (Fig. 5*c*), however, and is heavily concentrated in the target area of this fiber tract, the interpeduncular nucleus (Figs. 5*b,c*).
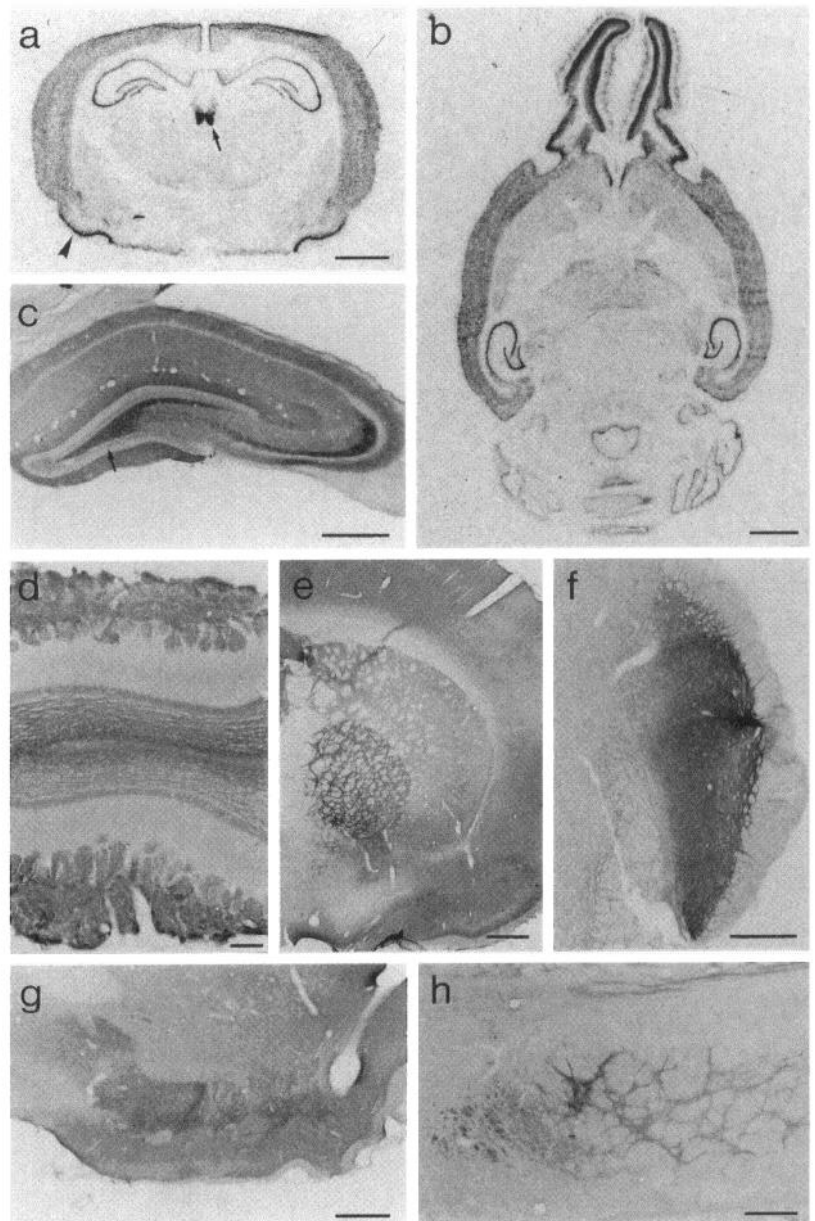
Figure 4. *Slo* mRNA and immunoreactivity in sections of the rat brain. *In situ* hybridizations of a coronary (*a*) and a horizontal (*b*) brain section incubated previously with an α-^{33}P-labeled probe complementary to *Slo* mRNA are shown. Note the high concentrations of *Slo* mRNA in the neocortex, especially in the outer layers of the piriform cortex (*arrowhead* in *a*), the habenula (*arrow* in *a*), hippocampus, olfactory bulb, and cerebellum. Photomicrographs of immunostained sections are shown for the hippocampus (*arrow* in *c* denotes faintly stained granule cell layer), olfactory bulb (*d*), striatum pallidum (*e*), substantia nigra (*f*), projection area of the medial forebrain bundle (*g*), and entopeduncular nucleus (*g*). Scale bars: *a, b,* 2 mm; *c, e–g,* 500 μm; *d, h,* 200 μm.

Taken together, these results of parallel immunocytochemistry and *in situ* hybridization provide compelling evidence that *Slo* is translated in neuronal somata (in which its mRNA is localized), but the protein is subsequently targeted to axons and their terminals.

Slo expression in the cerebellum

In the cerebellum, *Slo* mRNA is especially enriched in Purkinje cells and is found to a minor extent in the deep half of the molecular layer (mRNA: Figs. 3*a*, 4*b*, 5*f*; protein: Figs. 3*b*, 5*e*). In contrast to most other brain regions in which *Slo* channels are targeted into the axonal compartment, Purkinje cells show *Slo* protein expressed in their cell bodies and proximal dendritic trunk. To rule out the possibility that *Slo* channels are located in parallel with the voltage-gated K$^+$ channels Kv1.1 and Kv1.2 (McNamara et al., 1993; Sheng et al., 1994; Wang et al., 1994) in *pinceau* terminals (which are the axon collaterals of basket cells wrapping around the axon hillocks and initial axon segments of Purkinje cells), parallel sections were stained with a Kv1.2-specific

antibody (data not shown). These experiments enabled us to assign *Slo* immunoreactivity predominantly to Purkinje cell somata, whereas the Kv1.2 antibody revealed impressive staining of *pinceau* terminals and spared Purkinje cell somata. This is the only instance in which we observed *Slo* immunoreactivity mainly in a postsynaptic compartment.

In addition to *Slo* immunoreactivity in Purkinje cell somata, significant amounts of *Slo* immunoreactive protein (Figs. 3*b*, 5*h*) are contained in the deep cerebellar nuclei (which are a major projection area of the Purkinje cell axon). This could indicate that at least some Purkinje cell *Slo* channels are targeted into a presynaptic compartment (the deep cerebellar nuclei), whereas most of the *Slo* immunoreactivity seems to remain in the Purkinje cell somata, a localization of the channel that should be considered postsynaptic.

DISCUSSION

The distribution of the pore-forming α subunit of the maxi-K channel *Slo* has been determined by immunocytochemistry and *in*
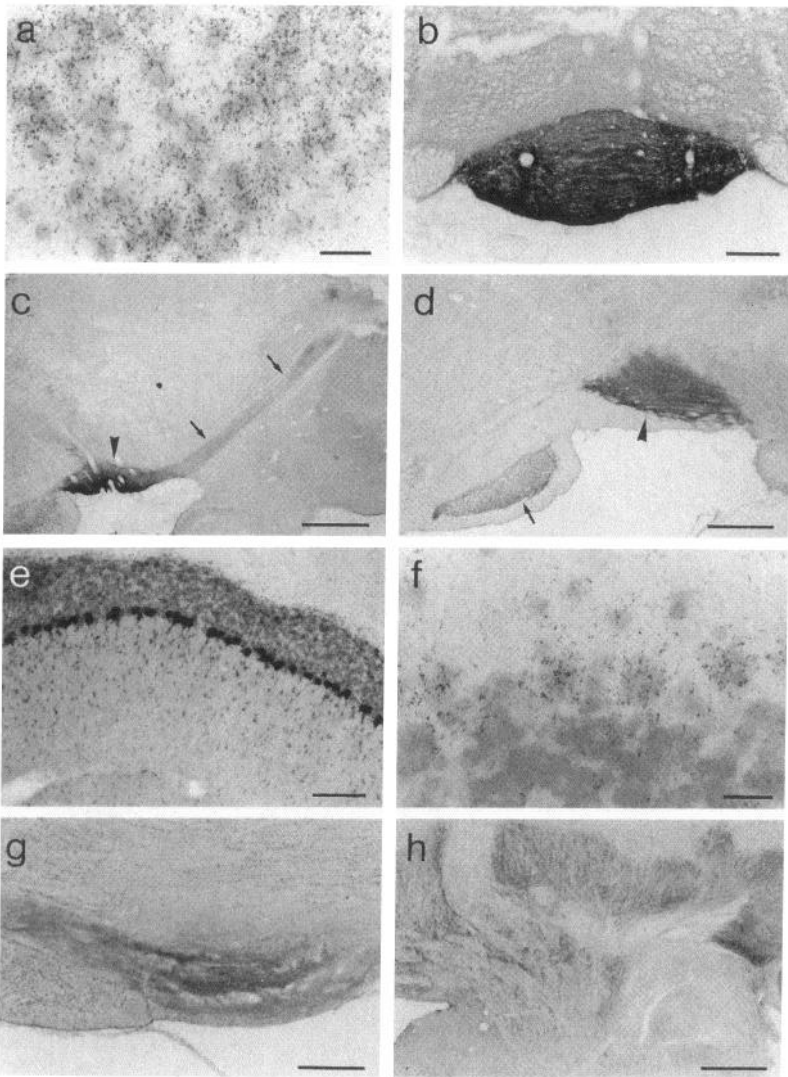
Figure 5. *Slo* mRNA and immunoreactivity in different areas of the rat brain. *Slo* immunoreactivity is shown for the fasciculus retroflexus (*c*, sagittal section, *arrows*) connecting the habenula (*Slo* mRNA in *a*) and the interpeduncular nucleus (*b* and *arrowheads* in *c*). Note the intensive staining in the pons (*arrow* in *d*, sagittal section) and substantia nigra *pars reticulata* (*arrowhead* in *d*). In cerebellar Purkinje cells, high concentrations of *Slo* immunoreactivity (*e*) and mRNA (*f*) were found. *Slo* immunoreactive staining also was seen in the pyramidal tract (*g*, sagittal section) and in the deep cerebellar nuclei (*h*, sagittal section). Scale bars: *c*, 1 mm; *d, g, h*, 500 μm; *b*, 200 μm; *a, f,* 25 μm.

situ hybridization in rat brain. For this purpose, a sequence-directed antibody (anti-$\alpha_{(913-926)}$) against a putative extracellular linker connecting two hydrophobic sequence stretches (S9 and S10) was raised. This antibody was designed to recognize all splice variants of *Slo* that have been described so far (Butler et al., 1993; Dworetzky et al., 1994; Pallanck and Ganetzky, 1994; Tseng-Crank et al., 1994). The specificity of this antibody was assessed in immunoblot experiments using membranes derived from micro-dissected brain areas. The *Slo* polypeptide is expressed in various brain regions as a diffuse staining protein of 125 kDa, probably consisting of multiple partially resolved components. The M_r of *Slo* in brain membranes is comparable with that obtained in other tissues that express *Slo* channels (bovine aorta and trachea and guinea-pig uterus) (Knaus et al., 1995). Taken together, these results provide compelling evidence that the 125 kDa polypeptide recognized by anti-$\alpha_{(913-926)}$ represents the gene product of *Slo* in rat brain, and they indicate that this antibody is a specific tool for studying *Slo* channels in brain tissue.

Despite the fact that [125I]ChTX has been used to identify maxi-K channels in different smooth muscle tissues (Vázquez et al., 1989) and that it has served as a marker for channel purification (Garcia-Calvo et al., 1994), the characterization of maxi-K channels in brain tissue with this ligand has not been possible. The reason for this could

be related to a relatively low density of maxi-K channels as compared with voltage-gated K+ channels to which [125I]ChTX binds with high affinity (Schweitz et al., 1989; Vázquez et al., 1990). Because IbTX is a selective blocker of maxi-K channels without affecting other ChTX-sensitive K+ channels (Galvez et al., 1990), we synthesized an IbTX analog IbTX-D19C, which was radiolabeled at position Cys[19] with *N*-[3H]ethylmaleimide. IbTX and IbTX-D19C block bilayer-reconstituted maxi-K channels with similar affinities and kinetics (O. McManus, personal communication). Thus, [3H]IbTX-D19C enabled us to investigate directly, for the first time, neuronal maxi-K channels in radioligand binding studies and to establish their pharmacological characteristics. The expression of maxi-K channels in various brain regions, as quantitated in radioligand binding studies with [3H]IbTX-D19C, was correlated closely with *Slo* expression levels determined by Western blotting. This prompted us to investigate the distribution of *Slo* immunoreactivity by immunocytochemistry and to determine the corresponding mRNA levels by *in situ* hybridization.

Anatomical and functional implications of distribution of neuronal *Slo* channels

Our study suggests a widespread distribution of *Slo*-immunoreactive perikarya and fibers as well as *Slo* mRNA in rat brain. The most

striking observation is that *Slo* expression is associated preferentially with major projection tracts (e.g., pyramidal tract, olfactory pathways, medial forebrain bundle, perforant path, mossy fibers, fasciculus retroflexus, and others), and that *Slo* immunoreactivity is especially enriched in terminal areas of these pathways. The high immunoreactivity within terminal areas and the fact that *Slo* mRNA is expressed in the same neurons clearly suggests a functional role of the maxi-K channel at the presynaptic nerve ending. In this respect, it is interesting to note that other K$^+$ channels (i.e., Kv1.1, Kv1.2, and Kv1.4) are also (at least partly) targeted to nerve terminals (Sheng et al., 1992, 1994; McNamara et al., 1993; Wang et al., 1994). In several brain areas (e.g., the hippocampal formation, the pallidum, and the substantia nigra), the distribution of the *Slo* protein overlays that of the A-type K$^+$ channel Kv1.4 (Sheng et al., 1992).

Voltage-gated K$^+$ channels such as Kv1.1, Kv1.2, and Kv1.4 do not depend on free intracellular Ca^{2+} for their activation. This property would allow them, when located presynaptically, to regulate spike duration and therefore the amount of neurotransmitter released. Maxi-K channels, however, require high Ca^{2+} concentrations (micromolar level) for their activation upon membrane depolarization (Tseng-Crank et al., 1994). Such high Ca^{2+} concentration could be achieved during high-frequency burst activities in presynaptic microdomains (e.g., near neurotransmitter release sites) (Llinas et al., 1992). In fact, experimental evidence suggests such a restricted localization of maxi-K channels at presynaptic nerve terminals (Robitaille and Charlton, 1992) in close proximity to voltage-gated Ca^{2+} channels (Gola and Crest, 1993; Robitaille et al., 1993). Such structural and functional coupling of *Slo* channels to voltage-gated Ca^{2+} channels could ensure high regional Ca^{2+} levels without causing cell damage, particularly when trains of action potentials are generated (Zucker, 1993). In this context, the maxi-K channel may serve as a depolarization-induced delimiter of high-frequency burst activities by hyperpolarizing the presynaptic membrane. This hyperpolarization would inactivate voltage-gated sodium and calcium channels, thereby blocking further propagation of action potentials. By this mechanism, maxi-K channels could counteract generalization of action potentials that occur during epileptic seizures, for example, and thus may represent a fast-responding and efficient rescue system at the presynaptic terminal.

It has been well documented that chronic intoxication with indole diterpenes, known to be the most selective nonpeptidyl blockers of maxi-K channels discovered to date (Knaus et al., 1994b), produces neurological disorders in ruminants. This intoxication is characterized by resting tremor, hyperexcitability, convulsions, ataxia, and tetanic seizures (Cole, 1980; Cole and Cox, 1981). The mechanism of action and moreover the precise neuroanatomical site(s) by which these tremorgens act are not understood (Selala et al., 1989). Some evidence, however, indicates altered neurotransmitter release (Norris et al., 1980; Peterson et al., 1982; Selala et al., 1991), which is consistent with a presynaptic localization of the mycotoxin-binding site. The intoxication symptoms could originate in the hippocampus and cerebral cortex (hyperexcitability, convulsions, and seizures) or in the basal ganglia and cerebellum (ataxia and tremor). All of these regions express high levels of *Slo* channels. Further investigation is needed to determine whether all symptoms are caused by maxi-K channel block, but given the anatomical distribution of this ion channel and the proven selectivity of these inhibitors, the findings could provide a preliminary insight into the physiological role of neuronal *Slo* channels.

REFERENCES

Adelman JP, Shen K-Z, Kavanaugh MP, Warren RA, Wu Y-N, Lagrutta A, Bond CT, North RA (1992) Calcium-activated potassium channels expressed from cloned complementary DNAs. Neuron 9:209–216.

Bradford MM (1976) A rapid and sensitive method for the quantitation of microgram quantities of protein utilizing the principle of protein-dye binding. Anal Biochem 72:248–254.

Butler A, Tsunoda S, McCobb DP, Wei A, Salkoff L (1993) mSlo, a complex mouse gene encoding "Maxi" calcium-activated potassium channels. Science 261:221–224.

Cole RJ (1980) Tremorgenic mycotoxins: an update. In: Antinutrients and natural toxins in foods (Ory RL, ed), pp 17–37. Westport, CT: Food and Nutrition.

Cole RJ, Cox RH (1981) Handbook of toxic fungal metabolites. New York: Academic.

DeLean A, Munson PJ, Rodbard D (1978) Simultaneous analysis of families of sigmoid curves: application to bioassays, radioligand assay and physiological dose-response curves. Am J Physiol 4:E97–E102.

Dworetzky SI, Trojnacki JT, Gribkoff VK (1994) Cloning and expression of a human large-conductance calcium activated potassium channel. Mol Brain Res 27:189–193.

Egan TM, Dagan D, Levitan IB (1993) Properties and modulation of calcium-activated potassium channels in rat olfactory bulb neurons. J Neurophysiol 69:1433–1442.

Galvez A, Gimenez-Gallego G, Reuben JP, Roy-Contancin L, Feigenbaum P, Kaczorowski GJ, Garcia ML (1990) Purification and characterization of a unique, potent, peptidyl probe for the high conductance calcium-activated potassium channel from venom of the scorpion *Buthus tamulus*. J Biol Chem 265:11083–11090.

Garcia-Calvo M, Knaus HG, McManus OB, Giangiacomo KM, Kaczorowski GJ, Garcia ML (1994) Purification and reconstitution of the high-conductance, calcium-activated potassium channel from trachea smooth muscle. J Biol Chem 269:676–682.

Garcia-Calvo M, Leonard RJ, Novick J, Stevens SP, Schmalhofer WA, Kaczorowski GJ, Garcia ML (1993) Purification, characterization, and biosynthesis of margatoxin, a component of *Centruroides margaritatus* venom that selectively inhibits voltage-dependent potassium channels. J Biol Chem 268:18866–18874.

Gola M, Crest M (1993) Colocalization of active K$_{Ca}$ channels and Ca^{2+} channels within Ca^{2+} domains of *Helix* neurons. Neuron 10:689–699.

Heimer L, Alheid GF, Zaborszky L (1995) Basal ganglia. In: The rat nervous system (Paxinos G, ed), pp 579–628. New York: Academic.

Johnson BA, Stevens SP, Williamson JM (1994) Determination of the three-dimensional structure of margatoxin by ^{1}H, ^{13}C, ^{15}N triple-resonance nuclear magnetic resonance spectroscopy. Biochemistry 33:15061–15070.

Knaus HG, Eberhart A, Koch ROA, Munujos P, Schmalhofer WA, Warmke JW, Kaczorowski GJ, Garcia ML (1995) Characterization of tissue-expressed α subunits of the high-conductance Ca^{2+}-activated K$^+$ channel. J Biol Chem 270:22434–22439.

Knaus HG, Garcia-Calvo M, Kaczorowski GJ, Garcia ML (1994a) Subunit composition of the high-conductance calcium-activated potassium channel from smooth muscle, a representative of the mSlo and slowpoke family of potassium channels. J Biol Chem 269:3921–3924.

Knaus HG, McManus OB, Lee SH, Schmalhofer WA, Garcia-Calvo M, Helms LMH, Sanchez M, Giangiacomo KM, Reuben JP, Smith III AB, Kaczorowski GJ, Garcia ML (1994b) Tremorgenic indole alkaloids potently inhibit smooth muscle high-conductance Ca^{2+}-activated K$^+$ channels. Biochemistry 33:5819–5828.

Laemmli UK (1970) Cleavage of structural proteins during the assembly of the head of the bacteriophage T4. Nature 227:680–685.

Lancaster B, Nicoll RA (1987) Properties of two calcium-activated hyperpolarizations in rat hippocampal neurons. J Physiol (Lond) 389:187–203.

Lancaster B, Nicoll RA, Perkel DJ (1991) Calcium activates two types of potassium channels in rat hippocampal neurons in culture. J Neurosci 11:23–30.

Latorre R, Oberhauser A, Labarca P, Alvarez O (1989) Varieties of calcium-activated potassium channels. Annu Rev Physiol 51:385–399.

Linden J (1982) Calculating the dissociation constant of an unlabeled compound from the concentration required to displace radioactive binding by 50%. J Cyclic Nucleotide Res 8:163–172.

Llinas R, Steinberg IZ, Walton K (1992) Presynaptic Ca^{2+} currents in squid giant synapse. Science 256:677–679.

MacDermott AB, Weight FF (1982) Action potential repolarization may involve a transient, Ca^{2+}-sensitive outward current in a vertebrate neuron. Nature 300:185–188.

Madison DV, Malenka RC, Nicoll RA (1991) Mechanisms underlying long-term potentiation of synaptic transmission. Annu Rev Neurosci 14:379–397.

Marksteiner J, Sperk G, Krause JE (1992) Distribution of neurons expressing neurokinin B in the rat brain: immunohistochemistry and *in situ* hybridization. J Comp Neurol 317:341–356.

McManus OB, Pallanck L, Helms LMH, Swanson R, Leonard RJ (1995) Functional role of the β subunit of high conductance Ca^{2+}-activated K^+ channels. Neuron 14:645–650.

McNamara NM, Muniz ZM, Wilkin GP, Dolly JO (1993) Prominent location of a K^+ channel containing the alpha subunit $K_v1.2$ in the basket cell nerve terminals of rat cerebellum. Neuroscience 57:1039–1045.

Meldrum BS, Corsellis JAN (1984) Epilepsy. In: Greenfield neuropathology (Adama JH, Corsellis JAN, Duchen LW, eds), pp 921–950. London: Edward Arnold.

Miller C, Moczydlowski E, Latorre R, Philips M (1985) Charybdotoxin, a protein inhibitor of single Ca^{2+}-activated K^+ channels from mammalian skeletal muscle. Nature 313:316–318.

Norris PJ, Smith CCT, De Belleroche J, Bradford HF, Mantle PG, Thomas AJ, Penny RHC (1980) Actions of tremorgenic fungal toxins on neurotransmitter release. J Neurochem 34:33–42.

Pallanck L, Ganetzky B (1994) Cloning and characterization of human and mouse homologs of the *Drosophila* calcium-activated potassium channel gene, *slowpoke*. Hum Mol Genet 3:1239–1243.

Paxinos G, Watson C (1986) The rat brain in stereotaxic coordinates. Sydney: Academic.

Peterson DW, Bradford HF, Mantle PG (1982) Actions of a tremorgenic mycotoxin on amino acid transmitter release in vivo. Biochem Pharmacol 31:2807–2810.

Reinhart PH, Chung S, Levitan IB (1989) A family of calcium-dependent potassium channels from rat brain. Neuron 2:1031–1041.

Reinhart PH, Chung S, Martin BL, Brautigan DL, Levitan IB (1991) Modulation of calcium-activated potassium channels from rat brain by protein kinase A and phosphatase 2A. J Neurosci 11:1627–1635.

Robitaille R, Charlton MP (1992) Presynaptic calcium signals and transmitter release are modulated by Ca^{2+}-activated K^+ channels. J Neurosci 12:297–305.

Robitaille R, Garcia ML, Kaczorowski GJ, Charlton MP (1993) Functional colocalization of calcium and calcium-gated potassium channels in control of neurotransmitter release. Neuron 11:645–655.

Schweitz H, Stansfeld CE, Bidard JN, Fagni L, Maes P, Lazdunski M (1989) Charybdotoxin blocks dendrotoxin-sensitive voltage-activated K^+ channels. FEBS Lett 250:519–522.

Selala MI, Daelemans F, Schepens PJC (1989) Fungal tremorgens: the mechanism of action of single nitrogen containing toxins—a hypothesis. Drug Chem Toxicol 12:237–257.

Selala MI, Laekeman GM, Loenders B, Masuku A, Herman AG, Schepens PJC (1991) In vitro effects of tremorgenic mycotoxins. J Nat Prod 54:207–212.

Sheng M, Tsaur ML, Jan YN, Jan LY (1992) Subcellular segregation of two A-type K^+ channel proteins in rat central neurons. Neuron 9:271–284.

Sheng M, Tsaur ML, Jan YN, Jan LY (1994) Contrasting subcellular localization of the Kv1.2 K^+ channel subunit in different neurons of rat brain. J Neurosci 14:2408–2417.

Sternberger L (1979) Immunohistochemistry. New York: Wiley.

Tseng-Crank J, Foster CD, Krause JD, Mertz R, Godinot N, DiChiara TJ, Reinhart PH (1994) Cloning, expression, and distribution of functionally distinct Ca^{2+}-activated K^+ channel isoforms from human brain. Neuron 13:1315–1330.

Vázquez J, Feigenbaum P, Katz G, King VF, Reuben JP, Roy-Contancin L, Slaughter RS, Kaczorowski GJ, Garcia ML (1989) Characterization of high affinity binding sites for charybdotoxin in sarcolemmal membranes from bovine aortic smooth muscle. J Biol Chem 264:20902–20909.

Vázquez J, Feigenbaum P, King VF, Kaczorowski GJ, Garcia ML (1990) Characterization of high affinity binding sites for charybdotoxin in synaptic plasma membranes from rat brain. J Biol Chem 265:15564–15571.

Wang H, Kunkel DD, Schwartzkroin PA, Tempel BL (1994) Localization of Kv1.1 and Kv1.2, two K channel proteins, to synaptic terminals, somata, and dendrites in the mouse brain. J Neurosci 14:4588–4599.

Wei A, Solaro C, Lingle CJ, Salkoff L (1994) Calcium sensitivity of BK-type K_{Ca} channels determined by a separable domain. Neuron 13:671–681.

Wisden WB, Morris BJ, Hunt SP (1990) *In situ* hybridization with synthetic probes. In: Molecular neurobiology: a practical approach (Chad J, Wheal H, eds), pp 205–225. Oxford: IRL.

Zalutsky RA, Nicoll RA (1990) Comparison of two forms of long-term potentiation in single hippocampal neurons. Science 248:1619–1624.

Zucker R (1993) Calcium and transmitter release. J Physiol (Lond) 87:25–36.